THE JOURNAL OF PHYSICAL CHEMISTRY Letters

Letter

pubs.acs.org/JPCL

Supervised Machine-Learning-Based Determination of Three-Dimensional Structure of Metallic Nanoparticles

Janis Timoshenko,*[,†] Deyu Lu,[‡] Yuewei Lin,[§] and Anatoly I. Frenkel*[,†,∥]

[†]Department of Material Science and Chemical Engineering, Stony Brook University, Stony Brook, New York 11794, United States
[‡]Center for Functional Nanomaterials, Brookhaven National Laboratory, Upton, New York 11973, United States
[§]Computational Science Initiative, Brookhaven National Laboratory, Upton, New York 11973, United States
[∥]Division of Chemistry, Brookhaven National Laboratory, Upton, New York 11973, United States

Supporting Information

ABSTRACT: Tracking the structure of heterogeneous catalysts under operando conditions remains a challenge due to the paucity of experimental techniques that can provide atomic-level information for catalytic metal species. Here we report on the use of X-ray absorption near-edge structure (XANES) spectroscopy and supervised machine learning (SML) for refining the 3D geometry of metal catalysts. SML is used to unravel the hidden relationship between the XANES features and catalyst geometry. To train our SML method, we rely on ab initio XANES simulations. Our approach allows one to solve the structure of a metal catalyst from its experimental XANES, as demonstrated here by reconstructing the average size, shape, and morphology of well-defined platinum nanoparticles. This method is applicable to the determination of the nanoparticle structure in operando studies and can be generalized to other nanoscale systems. It also allows on-the-fly XANES analysis and is a promising approach for high-throughput and time-dependent studies.

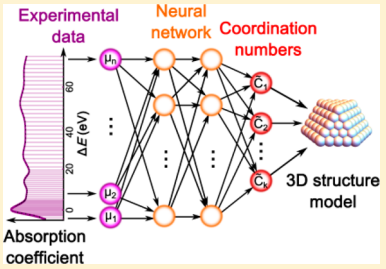

X-ray absorption spectroscopy (XAS) has been used for decades in studies of heterogeneous catalysts and nanostructured materials.[1,2] Its unique sensitivity to local atomistic structure around absorbing metal species[3,4] and the possibility to monitor in situ material transformations distinguish XAS as one of a very few experimental methods that can detect and analyze correlations of the structure of metallic nanoparticles (NPs) and their properties (e.g., catalytic activity).[5−10] This capability is a crucially needed step toward the goal of rational design of new catalysts.[11,12] In particular, average coordination numbers (CNs), extracted from extended X-ray absorption fine structure (EXAFS) for NPs in the ca. 3 nm size range and smaller, are widely used to determine particle sizes, structural motifs, and shapes in well-defined NPs. For NPs with narrow size and shape distributions, such analysis was required to link their average shape with their catalytic activity[6] and anomalous thermal properties[13,14] and monitor in situ the NP coarsening.[15]

Much less attention has been paid to the information encoded in X-ray absorption near-edge structure (XANES). The XANES portion of XAS spectrum is defined by electronic transitions to unoccupied atomic and hybridized (atom-ligand) states and is therefore sensitive to the details of 3D arrangements of atoms, providing sensitivity to structural and electronic characteristics.[5,16,17] XANES also is relatively less affected by structural disorder, which severely reduces the quality of EXAFS data and complicates their interpretation, especially for nanomaterials, where disorder is much more pronounced than in their bulk counterparts,[18−22] and also for in situ catalytic studies, which commonly involve high temperatures and hence result in strong thermal disorder. Finally, the better signal-to-noise ratio in XANES region in comparison with that in EXAFS region allows studies of more diluted samples in complex, X-rays attenuating sample environments and on strongly absorbing support materials, and also the reduction of the data acquisition times. The main challenge that hinders the usage of XANES for the quantitative analysis of nanocatalysts is the lack of a methodology that would allow one to extract structural characteristics ("descriptors") from the spectra (note, though, that for simple systems with a few degrees of freedom examples of such attempts are known[17,23−27]).

Recent advances in data-enabled discovery methods in chemical research[28,29] provide a key to this problem. In particular, supervised machine learning (SML) methods are a promising tool for establishing relations between spectral features and relevant descriptors of the investigated sample. Here we employ an SML method, namely, artificial neural network (NN), to unearth information about the 3D structure of nanoparticles from experimental XANES. An immediate challenge in this approach (as in any SML application) is the requirement to have a large representative, labeled training data set with thousands of data points. Clearly, it would be impractical to attempt to construct such data set from experimental measurements. Here we overcame this data

Received: September 6, 2017
Accepted: September 29, 2017
Published: September 29, 2017

DOI: 10.1021/acs.jpclett.7b02364
J. Phys. Chem. Lett. 2017, 8, 5091−5098

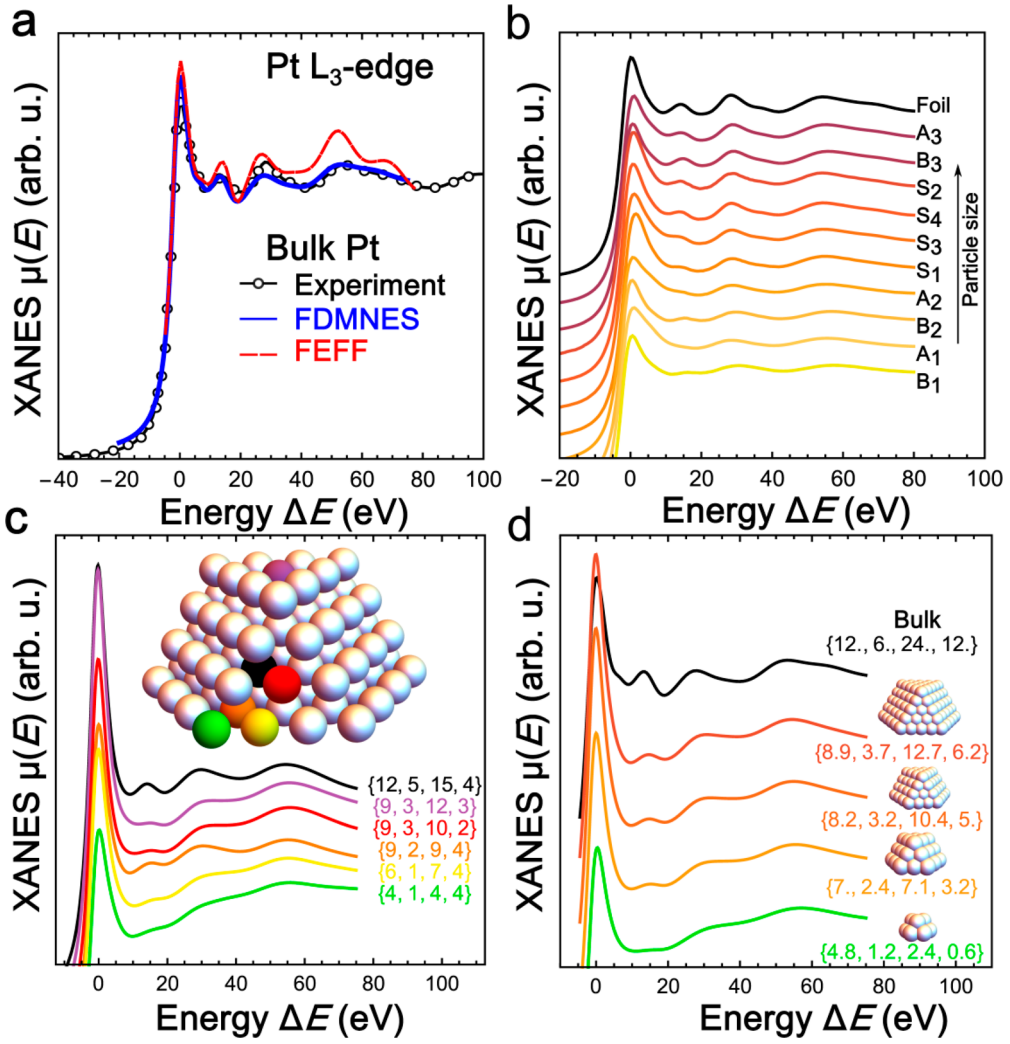

Figure 1. Size effect in Pt L_3-edge XANES spectra. (a) Experimental and theoretically calculated (with FEFF and FDMNES codes) spectra for Pt foil. (b) Experimental spectra for supported Pt NPs with different sizes, shifted vertically for clarity and ordered accordingly to average NPs size, as estimated from EXAFS and TEM analysis (particle size varies from ca. 0.9 to 2.9 nm). (c) Site-specific XANES spectra (shifted vertically for clarity), calculated with FDMNES code for sites with different first four CNs in a Pt NP, shown in the inset. (d) Particle-averaged CNs and averaged XANES spectra (shifted vertically for clarity), calculated with FDMNES code for Pt NPs of different sizes.

availability issue by constructing the training set via ab initio XANES simulations validated against experiment. By using theoretical simulations, we can generate a large number of spectra, corresponding to well-defined structure motifs.

We report the application of this method to the important problem of deciphering the 3D structure of supported platinum NPs. In our approach we use average CNs for the first few coordination shells $\{C_1, C_2, C_3, ...\}$ that are known to characterize the size and 3D shape of a nanoparticle with close-packed or nearly close-packed structure.[30] Next, we construct a training data set using ab initio codes FEFF[31] and FDMNES[32] (these codes are used interchangeably by the XAS community). We generate theoretical XANES $\mu^i(E)$ (here E is X-ray photon energy) for nanoparticles of different sizes/shapes, where the sets of corresponding average CNs are known. Artificial NN is then defined as a nonlinear function $h(\mu^i, \vec{\theta}) \rightarrow \{\tilde{C}_1, \tilde{C}_2, \tilde{C}_3, ...\}^i$ that uses as input a preprocessed and discretized XANES spectrum μ^i and returns a vector $\{\tilde{C}_1, \tilde{C}_2, \tilde{C}_3, ...\}^i$. As illustrated in the Supporting Information, Figure S1, function h can be represented as a network of nodes, where the values of the nodes in the first layer (input layer) are set by input vector μ^i, whereas the value of jth node in kth layer a_j^k is obtained as $a_j^k = f(\sum_m \theta_{j,m}^{k-1} a_m^{k-1})$. Here summation is carried out over all nodes in the $(k-1)$th layer, f is so-called activation function (hyperbolic tangent in our case), $\theta_{j,m}^k$ are NN parameters, and $\{\tilde{C}_1, \tilde{C}_2, \tilde{C}_3, ...\}$ are obtained as the values of a_j^k in the last (output) layer of NN. During the training process, we fit the NN parameters $\theta_{j,m}^k$ so that the distance between the true CNs vector $\{C_1, C_2, C_3, ...\}$ and NN output vector $\{\tilde{C}_1, \tilde{C}_2, \tilde{C}_3, ...\}$ is minimized for all spectra in our training set. After the optimal values of $\theta_{j,m}^k$ are found, NN can take experimental XANES as an input and determine $\{\tilde{C}_1, \tilde{C}_2, \tilde{C}_3, ...\}$ as estimators for average CNs for NPs in the corresponding sample. Knowing the CNs, one can then proceed to estimate the corresponding NPs size and shape, following the established prescription.[30] To avoid the averaging effects over a range of particle sizes/shapes, in this proof-of-

DOI: 10.1021/acs.jpclett.7b02364
J. Phys. Chem. Lett. 2017, 8, 5091−5098

principle work we focused on experimental data sets obtained for Pt nanoparticles with narrow size and shape distributions, as validated by previously reported EXAFS and TEM measurements.[13,14,33] We could therefore use the known results (NPs 3D geometry) for validating the quantitative capability of our new approach. Note that the current progress in the nanomaterial synthesis broadens significantly the availability of such monodisperse samples, and they have been widely used to establish relation between particle morphology and properties.[6,13,14] At the same time, possible applications of our method are not limited to such monodisperse systems only. For heterogeneous samples our method will yield ensemble-averaged CNs, and trends (rather than absolute values) in such averaged CNs can be used to monitor changes in particle shape and size.[15]

Sensitivity of XANES spectra to nanoparticle size and shape has been acknowledged theoretically previously,[16,34,35] and such an effect could be also recognized in our experimental spectra. In Figure 1a,b we show experimental Pt L_3-edge XANES spectra for Pt foil and Pt nanoparticles of different sizes on γ-Al_2O_3 support. Pt NPs were prepared via inverse micelle encapsulation method (samples S_1−S_4)[13] or by impregnation method (samples A_1−A_3),[14] and XANES spectra were acquired at room temperature in a H_2/He atmosphere. In addition, XANES spectra for samples A_1−A_3 were also acquired in a pure He atmosphere. These spectra are denoted as B_1−B_3. Differences in size (from ca. 0.9 nm to ca. 2.9 nm) and shape of these NPs were established previously based on their TEM and EXAFS data.[13,14,33] Details of sample preparation and experimental characterization are given in the Supporting Information. XANES changes upon increase in NPs size can be clearly observed in Figure 1b. In particular, all XANES features are smoother and less pronounced for particles of smaller size.

This effect can be qualitatively reproduced by ab initio XANES simulations, which is an important first indication that we can rely on such simulations to guide the analysis of NPs size and shape effect in experimental XANES data. In Figure 1d we compare XANES spectra, calculated with FDMNES code for Pt NPs of the same shape but different sizes. Note that the total XANES $\mu(E)$ of a nanoparticle is an average of partial contributions $\mu_j(E)$ from all N_a atoms in the nanoparticle: $\mu(E) = \sum_j \mu_j(E)/N_a$.[16,35] Therefore, in our simulations we first carry out independent XANES calculations for all NP sites and then average them. Such site-specific XANES spectra are shown in Figure 1c. As one can see, spectra for different sites differ significantly. Spectra for sites located deep in the NP core resemble those for bulk Pt material, whereas spectra for undercoordinated surface sites have significantly smoother features. The previously observed size sensitivity of particle-averaged XANES (Figure 1d) thus can be interpreted as a result of changes in the ratio of core sites and surface sites.

Each site can be conveniently characterized by site-specific CNs $\{c_1, c_2, c_3, ...\}$, that is, the total numbers of neighboring atoms in the first, second, third, and so on coordination shells of a particular site. Importantly, as shown in Figure 1c, the differences in the number of nearest neighbors only (c_1) cannot account for all of observed differences in site-specific spectra because the spectra for two nonequivalent sites with the same number of nearest neighbors (9) are clearly different. This demonstrates the sensitivity of XANES to the arrangements of more distant neighbors. The weights of different nonequivalent site-specific contributions to the total XANES are directly proportional to the ratios of nonequivalent sites and are related to the average CNs $\{C_1, C_2, C_3, ...\} = \sum_j \{c_1, c_2, c_3, ...\}_j/N_a$. Knowing the ratios of nonequivalent sites (or, alternatively, the set of average CNs), we can, in principle, reconstruct the 3D shape of the nanoparticle.

Extraction of this structural information from the particle-averaged XANES data is, however, challenging because, first, many such nonequivalent sites are present in nanoparticles, and the contrast between their partial contributions to the total spectrum is weak. Second, whereas ab initio simulations (which could be used to assign partial XANES contributions to specific NP sites) provide qualitative agreement with the experimental data, significant systematic errors of XANES modeling, as demonstrated in Figure 1a for Pt foil, prohibit in most cases the direct fitting via, for example, the least-squares procedure that has been used for simple systems.[17,23−27] In particular, note that the systematic error of Pt L_3-edge XANES modeling is comparable to the amplitude of broad XANES features for surface sites. Thus the contribution of surface sites cannot be analyzed reliably by linear methods.[36] The direct fitting of each experimental XANES spectrum would also be challenging due to high computational costs of ab initio XANES modeling (calculations of a XANES spectrum for a nanoparticle with a few hundreds of atoms may take several CPU hours).

The use of SML methods allows us to solve these problems. Such methods as artificial neural network approach can find complex, nonlinear relationships between features in XANES data and structure descriptors. The NN method can identify the spectral regions, relevant for structure determination, based on the information automatically extracted from the training on a vast number of training spectra, thus minimizing the influence of systematic errors.[37,38]

To establish relations between the features in averaged XANES $\mu(E)$ and average CNs $\{C_1, C_2, C_3, ...\}$, we train artificial NN with theoretical XANES data, calculated with FEFF and FDMNES codes for Pt particles of different sizes and shapes, shown in the Supporting Information, Figure S2. The pairs of theoretical spectra $\mu^i(E)$ and average CN sets $\{C_1, C_2, C_3, ...\}^i$ then can be used to fit the NN parameters $\theta^k_{j,m}$. Here and further below we limit our discussion to the analysis of the first four coordination shells only because the first four CNs are sufficient to represent the 3D shape and size of Pt nanoparticles and because atoms belonging to the first four coordination shells can be identified unambiguously not only in face-centered cubic (fcc)-type structures but also for icosahedral and hexagonal close-packed (hcp) structures,[30] which were also used for NN training. Details of our NN implementation and NN training are discussed in the Supporting Information. Note that the ab initio XANES calculations to construct the training data set were the most time-consuming part of our procedure and required several CPU days. Training of NN was accomplished in <1 h on a single CPU. Fortunately, for a given system both of these steps need to be performed only once. After the training is completed, NN can be used to analyze quickly an unlimited number of theoretical and experimental XANES spectra (the processing of each spectrum takes less than a second).

To validate our method, we provide as input for the trained NN with fixed parameters $\theta^k_{j,m}$ theoretical XANES spectra calculated for Pt NPs of different sizes and shapes with FEFF and FDMNES codes. The aim is to verify that the CNs

DOI: 10.1021/acs.jpclett.7b02364
J. Phys. Chem. Lett. 2017, 8, 5091−5098

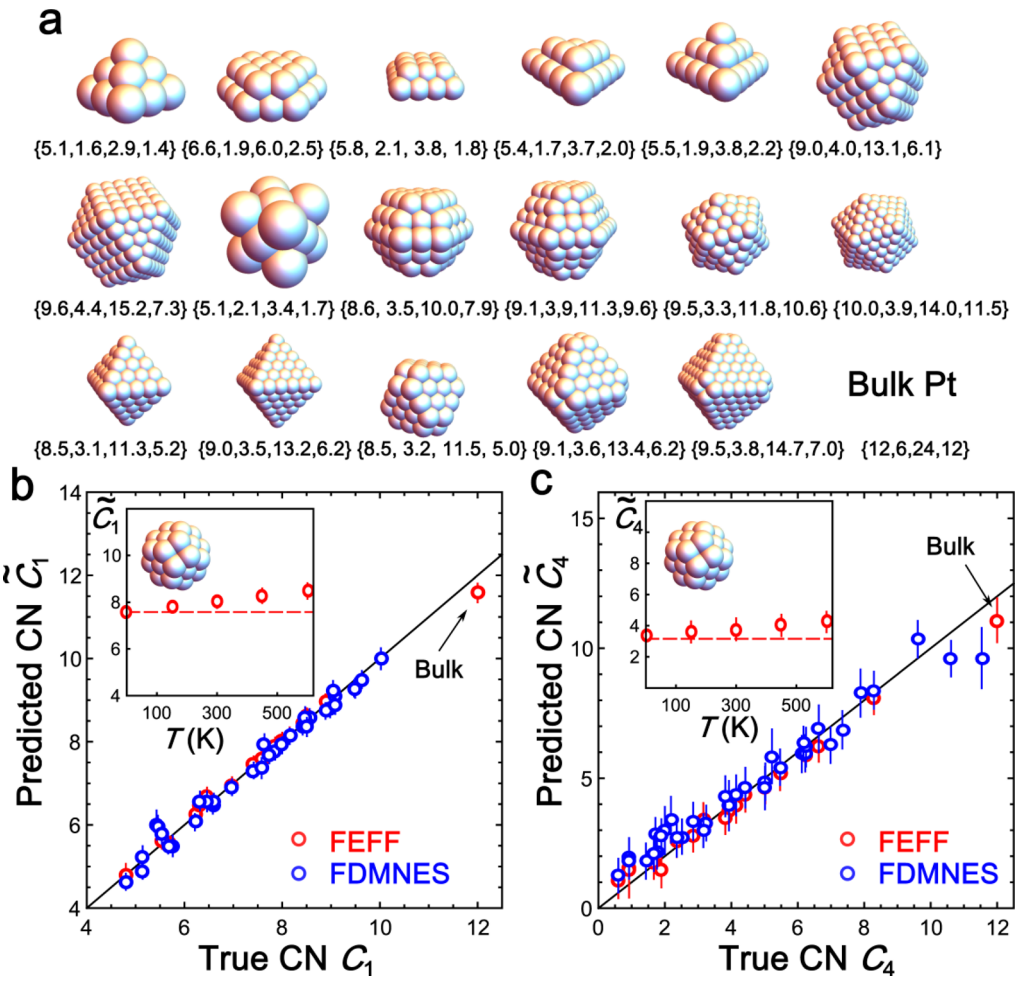

Figure 2. Validation of neural network using theoretical XANES data. (a) Additional Pt NPs models, used to validate the accuracy of trained NN. (b,c) True CNs for particles, shown in panel a and Figure S2a, are compared with the CNs, predicted by NN from XANES data, generated by FEFF or FDMNES codes. Solid lines are guides for eye. In the insets we show CNs, predicted by NN for truncated octahedral particle with 38 atoms from FEFF-generated XANES data, where thermal disorder was introduced using Debye model in the temperature range between 0 and 600 K. Debye temperature was set to bulk Pt value 244 K.[13] Horizontal dashed lines show the true value of corresponding CN.

$\{\tilde{C}_1, \tilde{C}_2, \tilde{C}_3, \tilde{C}_4\}$, predicted by NN, indeed are close to the true CN values $\{C_1, C_2, C_3, C_4\}$. For validation we use particle-averaged XANES data for particles that were used to construct training data set (Figure S2a) as well as for particles of other shapes and sizes (Figure 2a) with fcc-type structure, truncated by (100) and (111) planes, and also with icosahedral and hcp structures. The predicted and true first-shell and fourth-shell CNs for different NPs are compared in Figure 2b,c. Corresponding comparison for the second and third coordination shells is shown in the Supporting Information, Figure S3. In most cases the predicted CNs for all four coordination shells agree within error bars with the true values.

Special attention needs to be paid to disorder effects. It was demonstrated both experimentally and theoretically that atomic thermal motion results in small but detectable changes in XANES features.[39] Static disorder due to, for example, surface-induced stress in the material is also expected to have similar effect on XANES spectra. Note that the NN training was performed using XANES data for NPs models without any disorder in atomic positions. Therefore, to check how robust our analysis is with respect to the possible artifacts caused by disorder effects, we performed an additional validation of our method, providing FEFF-generated XANES spectra where thermal disorder was introduced via commonly used correlated Debye model[40] as input for our NN. The predicted CNs as a function of temperature are also shown in Figure 2b,c and in the Supporting Information, Figure S3. As one can see, the predicted CN values remain relatively stable in a broad range of temperatures (the changes in the predicted CNs values are comparable to the error bar of our analysis).

Next, we applied the NN to determine the CNs corresponding to experimental XANES[13,14] for Pt NPs on γ-Al_2O_3 and experimental Pt foil data. Obtained results for the first and fourth coordination shells are shown in Figure 3a,b, while those for the second and third coordination shells are in the Supporting Information, Figure S4.

As an important cross-check, we note that the first-shell CNs determined for all samples are in an excellent agreement with the results of EXAFS analysis (Figure 3a).[13,14] We can also observe a systematic increase in CNs with the increase in NP size, as estimated by TEM (Table 1). These findings demonstrate the validity of our NN/XANES method for the analysis of experimental data and that systematic differences between experimental and theoretical data used for NN training do not affect the performance of our method significantly.

DOI: 10.1021/acs.jpclett.7b02364
J. Phys. Chem. Lett. 2017, 8, 5091−5098

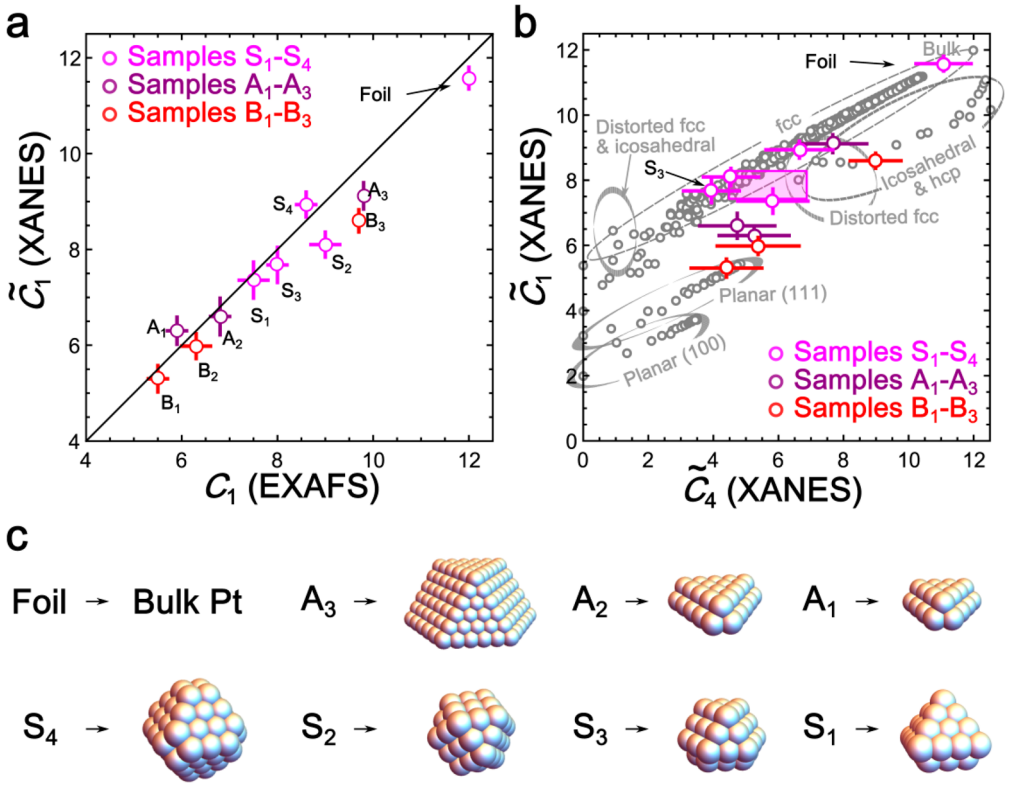

Figure 3. Coordination numbers predicted by NN from experimental XANES. (a) Comparison of the first-shell CNs, as predicted by NN method, and results of conventional EXAFS analysis for Pt NPs on γ-Al_2O_3; solid line is guide for eyes. (b) CNs, predicted by NN method for the fourth coordination shell. Gray empty circles correspond to CNs for Pt model clusters with different sizes and shapes, obtained from fcc-type Pt structure, truncated along (100) or (111) planes, as well as for clusters with icosahedral and hcp-type structures. Magenta rectangle in panel b shows the confidence region for CNs, obtained for sample S_3 from MS-EXAFS analysis in ref 13. (c) Corresponding possible 3D models of particles.

Table 1. Coordination Numbers, Predicted by NN from Experimental XANES for Pt Foil and Supported Pt NPs in a H_2/He Atmosphere

sample	$\tilde{C}_1$	$\tilde{C}_2$	$\tilde{C}_3$	$\tilde{C}_4$	d_{TEM} (nm)[a,b]	model NP CNs[c]	model NP size (nm)[c]
foil	11.6(2)	5.8(2)	23(1)	11.1(8)		{12, 6, 24, 12}	∞
A_3	9.1(3)	4.3(3)	11(2)	8(1)	3(1)	{9.4, 4.0, 14.4, 7.1}	2.8
S_4	8.9(3)	4.2(4)	10(2)	7(1)	1.2(2)	{8.5, 3.2, 11.5, 5.0}	1.2
S_2	8.1(3)	3.7(4)	8(2)	4.5(8)	1.2(3)	{7.8, 3.3, 9.6, 4.1}	1.1
S_3	7.7(4)	3.8(4)	4(2)	3.9(9)	0.9(2)	{7.7, 3.1, 9.2, 3.8}	1.1
S_1	7.4(4)	2.0(3)	3(1)	6(1)	1.1(2)	{7.4, 2.6, 8.0, 3.3}	1.2
A_2	6.6(4)	2.3(4)	3(1)	5(1)	1.1(3)	{6.6, 2.1, 6.0, 2.9}	1.4
A_1	6.3(3)	1.5(3)	2(1)	5(1)	0.9(2)	{6.2, 1.9, 5.1, 2.4}	1.1

[a]In the parentheses the uncertainty of the last digit is given. [b]Size of Pt NPs, determined by TEM.[13,14] [c]Coordination number and size of possible structure models, shown in Figure 3c.

Analysis of CNs for more distant coordination shells using EXAFS method is much less straightforward and less reliable due to a large number of structure parameters and multiple-scattering (MS) effects that need to be accounted for in the analysis.[41] Nevertheless, in Figure 3b and Figure S4 we show the results of such analysis, performed in ref 13, for sample S_3. CNs, predicted by NN, agree with the results of such MS-EXAFS analysis for the second and fourth coordination shells and are slightly smaller than the result from MS-EXAFS analysis for the third coordination shell.

Another indicator of the validity of our NN/XANES method is that for all samples we obtain physically reasonable sets of CNs. Note, as shown in Figure 3b and Figure S4, that CNs for different coordination shells are strongly correlated, and in a realistic cluster model one cannot expect to have, for example, very large CN for the fourth coordination shell while having small first-shell CN. The results yielded by our NN from experimental XANES data agree with this observation, and in almost all cases the obtained CNs agree reasonably with what could be expected for close-packed metallic particles with fcc-type structure.

Interestingly, when NN/XANES results for particles in H_2/He (spectra A_1–A_3) and pure He atmospheres (spectra B_1–B_3) are compared, slightly different CNs can be observed (see Figure 3a,b), suggesting changes in particle local structure. Whereas XANES data for samples in H_2/He suggested a well-ordered, fcc-type structure, more distorted structure models give better agreement with the obtained CNs for samples in a He atmosphere. This agrees with the observation that Pt interactions with hydrogen relieve the surface-induced strain in

DOI: 10.1021/acs.jpclett.7b02364
J. Phys. Chem. Lett. 2017, 8, 5091−5098

Pt NPs and result in more ordered particle structures.[13,14] This result demonstrates a utility of our method for the in situ studies of NPs shape and size changes in response to changes in ambient conditions.

For samples in H_2/He we used the CNs, predicted by our NN from experimental XANES, and information on NP size from TEM to propose a possible shape for investigated NPs (Table 1 and Figure 3c). Specifically, we selected structure models, whose first-shell CN within error bar agrees with the results of NN-XANES analysis and whose size within error bar agrees with TEM results; from this set we then selected models, whose second-, third-, and fourth-shell CNs are as close as possible to the results from NN-XANES analysis. We emphasize that we rely here on the a priori TEM observation that the NP size and shape distribution in all of these samples is narrow. Note that the influence of NP size distribution on CNs, derived from EXAFS analysis, is discussed in ref 42, where it was demonstrated that broad size distribution may result in CN overestimation. The analysis of CNs in this case will yield an effective (median) shape of the cluster.[42] The same arguments are also applicable for XANES analysis results. Note also that, of course, for each sample at least several similar NPs models can be found (see the Supporting Information, Figure S5), which all agree reasonably with the predictions of NN/XANES method. The larger the particle, the larger the number of different structure models that fit the obtained CNs. As with any other XAS method, also for our NN/XANES approach all particles with sizes larger than ca. 5 nm will be indistinguishable from bulk material because the fraction of undercoordinated surface sites gets negligible, and the spectra for sites in the NPs core are close to XANES of bulk metal. Therefore, the NP structure models, shown in Figure 3c, should be considered only as representative examples of possible structures. Nevertheless, one can note that the shapes, predicted here by our NN/XANES method, are in agreement with the shapes, proposed from advanced MS-EXAFS and TEM size analysis.[13]

As an independent reality check, we validated the so-obtained, representative NPs shapes with reverse Monte Carlo (RMC) simulations of EXAFS data. In RMC-EXAFS analysis the structure models that were established based on our NN/XANES method were used to calculate the corresponding theoretical EXAFS spectra, allowing small deviations from the initial structure to account for the disorder effects.[19,43] In Supporting Information Figure S6 we demonstrate that RMC-EXAFS simulations for all structure models yielded by NN/XANES method confirm their agreement with the available EXAFS data. More details of the RMC-EXAFS method are given in the Supporting Information.

Overall, our NN/XANES analysis shows that whereas the inverse micelle encapsulation method results in more spherical, symmetric particles,[44] the particles prepared via impregnation method have flat, raft-like shapes. In both cases smaller particles have more flattened shapes due to a strong interaction of Pt atoms with the support.[44] This finding demonstrates the utility of our method for determination of catalyst morphology and enables, for example, direct correlation of NP shape with its catalytic properties. We emphasize here again that the determination of particle shape, as developed here on the basis of XANES data, relies on the use of samples with narrow particle size and shape distributions (the same requirement as for the use of EXAFS modeling methods developed previously for the same purpose), as validated, for example, by TEM imaging. Note, however, that also in the cases when the particle size and shape distribution is not narrow, the ability provided by our method to obtain ensemble average (effective) CNs and, importantly, to monitor in situ the changes in such effective CNs can significantly advance our understanding of particle formation, coarsening, and agglomeration processes, despite the fact that in this case the absolute CN values will be somewhat overestimated. For example, increase in all CNs can be unambiguously interpreted as evidence of NP growth. Similarly, increase in some CNs while others are decreasing indicates changes in NP shape. Also, as emphasized above, after NN training is complete for a specific chemical element we can use the so obtained NN as a static analysis tool to quickly find corresponding structures for an unlimited number of experimental XANES spectra in nanoparticles consisting of those atomic species. Furthermore, such analysis can be even done on-the-fly during the data acquisition, which is a unique capability for in situ studies. The ability of our method to analyze quickly a large number of XANES spectra makes it also attractive for high-throughput studies, which are getting progressively more widespread with the development of the new generation of X-ray sources that provide unprecedented photon flux and dramatically reduce the spectra acquisition time.[45,46]

In summary, using a sample set of well-defined metal nanoparticles with size and shape control as an example, we have demonstrated that XANES spectra in nanostructures can be translated into real-space information about the coordination environment of metal atoms. Only by using neural networks was it possible to extend the sensitivity of this technique to the fourth coordination shell and thus to enable the determination of particle sizes and shapes. Unlike MS-EXAFS or RMC-EXAFS methods, our XANES-based approach does not require high-quality EXAFS data and thus makes possible advanced analysis of NPs structure at high temperatures, with diluted samples on X-rays absorbing supports and in complex sample environments. Whereas we have focused here on the study of metal nanoparticles, our method can be easily extended to other nanoscale systems. We expect it will be especially beneficial to analyze the in situ changes in the environments of metal atoms in a wide range of catalytically relevant systems and processes.

■ ASSOCIATED CONTENT

Supporting Information

The Supporting Information is available free of charge on the ACS Publications website at DOI: 10.1021/acs.jpclett.7b02364.

Schematic representation of artificial neural network-based method for prediction of nanoparticle size and shape; details of sample preparation and experimental characterization; details of ab initio calculations of XANES spectra; details of supervised machine learning implementation and training; cluster models and theoretical XANES data for neural network training; validation of neural network using theoretical XANES data (2nd and 3rd coordination shells); coordination numbers predicted by neural network from experimental XANES (2nd and 3rd coordination shells); additional examples of structure models that have CNs and sizes close to those estimated by neural network-based analysis of experimental XANES data and TEM analysis; details of RMC-EXAFS analysis; and validation of Pt NPs 3D

DOI: 10.1021/acs.jpclett.7b02364
J. Phys. Chem. Lett. 2017, 8, 5091−5098

shapes, determined by the NN/XANES method, with RMC-EXAFS simulations. (PDF)

AUTHOR INFORMATION

Corresponding Authors

*J.T.: E-mail: Janis.timosenko@stonybrook.edu.
*A.I.F.: E-mail: anatoly.frenkel@stonybrook.edu.

ORCID

Yuewei Lin: 0000-0002-1429-4543
Anatoly I. Frenkel: 0000-0002-5451-1207

Notes

The authors declare no competing financial interest.

ACKNOWLEDGMENTS

A.I.F.'s work was funded by the Division of Chemical Sciences, Geosciences, and Biosciences, Office of Basic Energy Sciences of the U.S. Department of Energy through Grant DE-FG02-03ER15476. D.L. used resources of the Center for Functional Nanomaterials, which is a U.S. DOE Office of Science Facility, at Brookhaven National Laboratory under Contract No. DE-SC0012704. Y.L. gratefully acknowledges the support by BNL LDRD 16-039. RMC-EXAFS simulations were performed on the LASC cluster-type computer at Institute of Solid State Physics of the University of Latvia. X-ray absorption spectra for Pt nanoparticles used in this work (also published in refs 13,14) were obtained at the beamline 33BM-B of Advanced Photon Source at Argonne National Laboratory and beamline X18B of National Synchrotron Light Source of Brookhaven National Laboratory. We are grateful to S. Yoo for valuable discussions.

REFERENCES

(1) Frenkel, A. Solving the 3D structure of metal nanoparticles. *Z. Kristallogr. - Cryst. Mater.* **2007**, *222*, 605−611.
(2) Frenkel, A. I. Applications of extended X-ray absorption fine-structure spectroscopy to studies of bimetallic nanoparticle catalysts. *Chem. Soc. Rev.* **2012**, *41*, 8163−8178.
(3) Billinge, S. J. L.; Levin, I. The problem with determining atomic structure at the nanoscale. *Science* **2007**, *316*, 561−565.
(4) Rehr, J. J.; Albers, R. C. Theoretical approaches to X-ray absorption fine structure. *Rev. Mod. Phys.* **2000**, *72*, 621−654.
(5) Frenkel, A. I.; Rodriguez, J. A.; Chen, J. G. Synchrotron techniques for in situ catalytic studies: capabilities, challenges, and opportunities. *ACS Catal.* **2012**, *2*, 2269−2280.
(6) Mostafa, S.; Behafarid, F.; Croy, J. R.; Ono, L. K.; Li, L.; Yang, J. C.; Frenkel, A. I.; Cuenya, B. R. Shape-dependent catalytic properties of Pt nanoparticles. *J. Am. Chem. Soc.* **2010**, *132*, 15714−15719.
(7) Paredis, K.; Ono, L. K.; Mostafa, S.; Li, L.; Zhang, Z.; Yang, J. C.; Barrio, L.; Frenkel, A. I.; Cuenya, B. R. Structure, chemical composition, and reactivity correlations during the in situ oxidation of 2-propanol. *J. Am. Chem. Soc.* **2011**, *133*, 6728−6735.
(8) Frenkel, A. I.; Small, M. W.; Smith, J. G.; Nuzzo, R. G.; Kvashnina, K. O.; Tromp, M. An in situ study of bond strains in 1 nm Pt catalysts and their sensitivities to cluster−support and cluster−adsorbate interactions. *J. Phys. Chem. C* **2013**, *117*, 23286−23294.
(9) Bare, S. R.; Ressler, T. Characterization of catalysts in reactive atmospheres by X-ray absorption spectroscopy. *Adv. Catal.* **2009**, *52*, 339−465.
(10) Bordiga, S.; Groppo, E.; Agostini, G.; van Bokhoven, J. A.; Lamberti, C. Reactivity of surface species in heterogeneous catalysts probed by in situ X-ray absorption techniques. *Chem. Rev.* **2013**, *113*, 1736−1850.
(11) Norskov, J. K.; Bligaard, T.; Rossmeisl, J.; Christensen, C. H. Towards the computational design of solid catalysts. *Nat. Chem.* **2009**, *1*, 37−46.
(12) Ulissi, Z. W.; Medford, A. J.; Bligaard, T.; Norskov, J. K. To address surface reaction network complexity using scaling relations machine learning and DFT calculations. *Nat. Commun.* **2017**, *8*, 14621.
(13) Cuenya, B. R.; Frenkel, A.; Mostafa, S.; Behafarid, F.; Croy, J.; Ono, L.; Wang, Q. Anomalous lattice dynamics and thermal properties of supported size-and shape-selected Pt nanoparticles. *Phys. Rev. B: Condens. Matter Mater. Phys.* **2010**, *82*, 155450.
(14) Sanchez, S. I.; Menard, L. D.; Bram, A.; Kang, J. H.; Small, M. W.; Nuzzo, R. G.; Frenkel, A. I. The emergence of nonbulk properties in supported metal clusters: negative thermal expansion and atomic disorder in Pt nanoclusters supported on γ-Al_2O_3. *J. Am. Chem. Soc.* **2009**, *131*, 7040−7054.
(15) Matos, J.; Ono, L.; Behafarid, F.; Croy, J.; Mostafa, S.; DeLaRiva, A.; Datye, A.; Frenkel, A.; Cuenya, B. R. In situ coarsening study of inverse micelle-prepared Pt nanoparticles supported on γ-Al_2O_3: pretreatment and environmental effects. *Phys. Chem. Chem. Phys.* **2012**, *14*, 11457−11467.
(16) Ankudinov, A.; Rehr, J.; Low, J. J.; Bare, S. R. Sensitivity of Pt X-ray absorption near edge structure to the morphology of small Pt clusters. *J. Chem. Phys.* **2002**, *116*, 1911−1919.
(17) Bugaev, A. L.; Guda, A. A.; Lazzarini, A.; Lomachenko, K. A.; Groppo, E.; Pellegrini, R.; Piovano, A.; Emerich, H.; Soldatov, A. V.; Bugaev, L. A.; et al. In situ formation of hydrides and carbides in palladium catalyst: when XANES is better than EXAFS and XRD. *Catal. Today* **2017**, *283*, 119−126.
(18) Chill, S. T.; Anderson, R. M.; Yancey, D. F.; Frenkel, A. I.; Crooks, R. M.; Henkelman, G. Probing the limits of conventional extended X-ray absorption fine structure analysis using thiolated gold nanoparticles. *ACS Nano* **2015**, *9*, 4036−4042.
(19) Timoshenko, J.; Frenkel, A. I. Probing structural relaxation in nanosized catalysts by combining EXAFS and reverse Monte Carlo methods. *Catal. Today* **2017**, *280*, 274−282.
(20) Yevick, A.; Frenkel, A. I. Effects of surface disorder on EXAFS modeling of metallic clusters. *Phys. Rev. B: Condens. Matter Mater. Phys.* **2010**, *81*, 115451.
(21) Clausen, B. S.; Norskov, J. K. Asymmetric pair distribution functions in catalysts. *Top. Catal.* **2000**, *10*, 221−230.
(22) Witkowska, A.; Di Cicco, A.; Principi, E. Local ordering of nanostructured Pt probed by multiple-scattering XAFS. *Phys. Rev. B: Condens. Matter Mater. Phys.* **2007**, *76*, 104110.
(23) Benfatto, M.; Congiu-Castellano, A.; Daniele, A.; Della Longa, S. MXAN: a new software procedure to perform geometrical fitting of experimental XANES spectra. *J. Synchrotron Radiat.* **2001**, *8*, 267−269.
(24) Della Longa, S.; Arcovito, A.; Girasole, M.; Hazemann, J.; Benfatto, M. Quantitative analysis of X-ray absorption near edge structure data by a full multiple scattering procedure: the Fe-CO geometry in photolyzed carbonmonoxy-myoglobin single crystal. *Phys. Rev. Lett.* **2001**, *87*, 155501.
(25) Smolentsev, G.; Soldatov, A.; Feiters, M. Three-dimensional local structure refinement using a full-potential XANES analysis. *Phys. Rev. B: Condens. Matter Mater. Phys.* **2007**, *75*, 144106.
(26) van der Veen, R. M.; Kas, J. J.; Milne, C. J.; Pham, V.-T.; El Nahhas, A.; Lima, F. A.; Vithanage, D. A.; Rehr, J. J.; Abela, R.; Chergui, M. L-edge XANES analysis of photoexcited metal complexes in solution. *Phys. Chem. Chem. Phys.* **2010**, *12*, 5551−5561.
(27) Zhan, F.; Tao, Y.; Zhao, H. Alternative difference analysis scheme combining R-space EXAFS fit with global optimization XANES fit for X-ray transient absorption spectroscopy. *J. Synchrotron Radiat.* **2017**, *24*, 818−824.
(28) Montavon, G.; Rupp, M.; Gobre, V.; Vazquez-Mayagoitia, A.; Hansen, K.; Tkatchenko, A.; Müller, K.-R.; von Lilienfeld, O. A. Machine learning of molecular electronic properties in chemical compound space. *New J. Phys.* **2013**, *15*, 095003.
(29) Ramakrishnan, R.; Dral, P. O.; Rupp, M.; von Lilienfeld, O. A. Big data meets quantum chemistry approximations: the Δ-machine learning approach. *J. Chem. Theory Comput.* **2015**, *11*, 2087−2096.
(30) Glasner, D.; Frenkel, A. I. Geometrical characteristics of regular polyhedra: application to EXAFS studies of nanoclusters. *AIP Conf. Proc.* **2007**, *882*, 746−748.

DOI: 10.1021/acs.jpclett.7b02364
J. Phys. Chem. Lett. 2017, 8, 5091−5098

(31) Rehr, J. J.; Kas, J. J.; Vila, F. D.; Prange, M. P.; Jorissen, K. Parameter-free calculations of X-ray spectra with FEFF9. *Phys. Chem. Chem. Phys.* **2010**, *12*, 5503−5513.
(32) Bunău, O.; Joly, Y. Self-consistent aspects of X-ray absorption calculations. *J. Phys.: Condens. Matter* **2009**, *21*, 345501.
(33) Roldan Cuenya, B.; Croy, J. R.; Mostafa, S.; Behafarid, F.; Li, L.; Zhang, Z.; Yang, J. C.; Wang, Q.; Frenkel, A. I. Solving the structure of size-selected Pt nanocatalysts synthesized by inverse micelle encapsulation. *J. Am. Chem. Soc.* **2010**, *132*, 8747−8756.
(34) Ankudinov, A.; Rehr, J.; Low, J.; Bare, S. Theoretical interpretation of XAFS and XANES in Pt clusters. *Top. Catal.* **2002**, *18*, 3−7.
(35) Bazin, D.; Sayers, D.; Rehr, J.; Mottet, C. Numerical simulation of the platinum LIII edge white line relative to nanometer scale clusters. *J. Phys. Chem. B* **1997**, *101*, 5332−5336.
(36) Timoshenko, J.; Shivhare, A.; Scott, R. W. J.; Lu, D. Y.; Frenkel, A. I. Solving local structure around dopants in metal nanoparticles with ab initio modeling of X-ray absorption near edge structure. *Phys. Chem. Chem. Phys.* **2016**, *18*, 19621−19630.
(37) Bhadeshia, H. K. D. H. Neural networks in materials science. *ISIJ Int.* **1999**, *39*, 966−979.
(38) Kuno, A.; Matsuo, M. Nondestructive speciation of solid mixtures by multivariate calibration of X-ray absorption near-edge structure using artificial neural networks and partial least-squares. *Anal. Sci.* **2000**, *16*, 597−602.
(39) Vila, F.; Rehr, J.; Kas, J.; Nuzzo, R.; Frenkel, A. Dynamic structure in supported Pt nanoclusters: real-time density functional theory and X-ray spectroscopy simulations. *Phys. Rev. B: Condens. Matter Mater. Phys.* **2008**, *78*, 121404.
(40) Rehr, J.; Ankudinov, A. Progress in the theory and interpretation of XANES. *Coord. Chem. Rev.* **2005**, *249*, 131−140.
(41) Frenkel, A. I. Solving the structure of nanoparticles by multiple-scattering EXAFS analysis. *J. Synchrotron Radiat.* **1999**, *6*, 293−295.
(42) Frenkel, A. I.; Yevick, A.; Cooper, C.; Vasic, R. Modeling the structure and composition of nanoparticles by extended X-ray absorption fine-structure spectroscopy. *Annu. Rev. Anal. Chem.* **2011**, *4*, 23−39.
(43) Timoshenko, J.; Anspoks, A.; Kalinko, A.; Kuzmin, A. Local structure of nanosized tungstates revealed by evolutionary algorithm. *Phys. Status Solidi A* **2015**, *212*, 265−273.
(44) Cuenya, B. R.; Ortigoza, M. A.; Ono, L.; Behafarid, F.; Mostafa, S.; Croy, J.; Paredis, K.; Shafai, G.; Rahman, T.; Li, L.; et al. Thermodynamic properties of Pt nanoparticles: Size, shape, support, and adsorbate effects. *Phys. Rev. B: Condens. Matter Mater. Phys.* **2011**, *84*, 245438.
(45) Tsapatsaris, N.; Beesley, A. M.; Weiher, N.; Tatton, H.; Dent, A. J.; Mosselmans, F. J.; Tromp, M.; Russu, S.; Evans, J.; Harvey, I.; et al. High throughput in situ XAFS screening of catalysts. *AIP Conf. Proc.* **2007**, *882*, 597−599.
(46) Grunwaldt, J.-D.; Frenkel, A. I. Synchrotron studies of catalysts: from XAFS to QEXAFS and beyond. *Synchrotron Radiat. News* **2009**, *22*, 2−4.

DOI: 10.1021/acs.jpclett.7b02364
J. Phys. Chem. Lett. 2017, 8, 5091−5098